energies

MDPI

Article

Improving Thermal Stability of Perovskite Solar Cells by Thermoplastic Additive Engineering

Zaheen Uddin [1], Junhui Ran [1,*], Elias Stathatos [2] and Bin Yang [1,*]

[1] College of Materials Science and Engineering, Hunan University, Changsha 410082, China
[2] Nanotechnology & Advanced Materials Laboratory, Department of Electrical and Computer Engineering, University of the Peloponnese, 26334 Patras, Greece
* Correspondence: jhran@hnu.edu.cn (J.R.); yangb1@hnu.edu.cn (B.Y.)

Abstract: The commercialization of perovskite solar cells is hindered by the poor thermal stability of organic–inorganic hybrid perovskite materials. Herein, we demonstrate that crystalline thermoplastic polymer additives, such as a mixture of polyethylene oxide (PEO, 100,000 MW) and polyethylene glycol (PEG, 12,000 MW), can improve the thermal stability of $CH_3NH_3PbI_3$ ($MAPbI_3$) perovskites and thereby enhance device stability. High-quality less-defect perovskite films were obtained by establishing a strong reaction between hydroxy groups in the PEO + PEG mixture and the uncoordinated Pb^{2+} in $MAPbI_3$ perovskites, leading to a high power conversion efficiency of over 18% despite the presence of insulating thermoplastic polymers in the $MAPbI_3$ film. More importantly, as compared with pristine $MAPbI_3$ perovskite solar cells, the PEO + PEG-modified counterparts showed significantly improved stability under thermal treatment at 85 °C in ambient air with a relative humidity of 50–60%, remaining at nearly 71% of their initial efficiency values after 120 h. These demonstrations offer a feasible thermoplastic polymer additive engineering strategy to improve the thermal stability of perovskite solar cells.

Keywords: halide perovskites; thermal stability; thermoplastic additives; solar cells

Citation: Uddin, Z.; Ran, J.; Stathatos, E.; Yang, B. Improving Thermal Stability of Perovskite Solar Cells by Thermoplastic Additive Engineering. *Energies* **2023**, *16*, 3621. https://doi.org/10.3390/en16093621

Academic Editors: Peter D. Lund and Jeff Kettle

Received: 4 March 2023
Revised: 19 April 2023
Accepted: 20 April 2023
Published: 22 April 2023

1. Introduction

Organic–inorganic hybrid perovskite solar cells (PSCs) have been a key field of research in the previous decade due to their high light absorption coefficient, varied bandgap, and long carrier lifetime [1–4]. Owning to their remarkable photovoltaic performance and low-cost fabrication, organic–inorganic halide PSCs have tremendous potential as a foundation for the next generation of photovoltaics. In a relatively short development period, PSCs have achieved a startling 25.7% power conversion efficiency (PCE) due to their optoelectronic characteristics [5–9]. The key to this fast development is the groundbreaking thin-film technology that has been established. Although the efficiency of PSCs has immensely shortened the gap with the Schockley–Quisser theoretical limit, there are numerous interior and surface defects in perovskites caused by their polycrystalline structure, volatile organic components, and ionic nature, generating very limited device stability that prevents them from being commercialized [10–12]. This is certainly relevant for devices subjected to environmental stress, such as humidity, heat, oxygen, sunlight, and combinations of these, all recognized as possible degradation factors [13–16]. Therefore, developing ultra-stable and high-efficiency devices that can withstand harsh operating conditions is a challenging task and an urgent need.

Organic–inorganic hybrid perovskites easily decompose in both humid and hot environments [17,18]. Improvements in stability against humidity have been reported in several studies. The humid environments' stability issue can be simply solved by reliable encapsulation [19], which is very mature in the industry. However, thermal stability is not such a case. Despite this, industrial validation needs exceptional temperature stability, which

cannot be achieved by encapsulation. The hybrid perovskites usually decompose under substantial heating due to the intrinsic volatile capability of organic components which are only weakly bound with inorganic PbI_6 frameworks. Therefore, it is of great importance to develop feasible approaches to improve the thermal stability of organic–inorganic hybrid perovskites. Researchers in the field of organic–inorganic hybrid perovskites are striving to develop various mechanisms and strategies that can improve their photovoltaic performance. In order to minimize barriers towards the commercialization of organic–inorganic hybrid perovskite solar cells, compositional engineering, the incorporation of additives, the interface and surface passivation of light absorber layers, the selection of charge transport layers, solvent engineering, and electrode layer selection have received much attention [20–23].

Additive engineering has been extensively studied for improving device stability [24–26]. Additive engineering is viewed as a promising option to form defect-free perovskite crystals. The addition of additives to the perovskite precursor solutions was found to be advantageous for passivating bulk and grain boundary defects during the formation of the perovskite phase [27,28]. For example, an additive of oxalic acid (OA) containing two bifacial carboxylic acid groups was added to the perovskite precursor solution to enlarge grain size, reduce grain boundaries, and passivate trap states, resulting in a higher power conversion efficiency and excellent thermal stability [29]. Moreover, potassium hexafluorophosphate (KPF_6) as a modifier was employed to accelerate perovskite crystallization by boosting completely coordinated intermediate groups in the solution and compensating for halide vacancies, which passivated ionic defects and decreased non-radiative recombination, strengthening device efficiency and stability [30]. Li et al. demonstrated that the crosslinking between CH_2=CH groups in dipentaerythritol pentaacrylate (DPPA) blocks ion migration channels at grain boundaries [31]. Therefore, due to its synergistic function, ion migration was effectively inhibited while the PSCs demonstrated strong operating stability. In addition, polymeric materials can act as growth templates and retardants to form high-quality perovskite films [32,33]. Lee et al. investigated the use of a non-ionic surfactant, polyoxyethylene (20) sorbitan monolaurate (Tween 20), to enhance the performance and stability of perovskite solar cells fabricated using the thermal-assisted blade-coating method. They demonstrated that adding an appropriate amount of Tween 20 to a $MAPbI_3$ perovskite film can control the crystalline domain size and significantly enhance radiative recombination, resulting in a high power conversion efficiency [34]. Despite their high molecular weights, the polymers remained within the perovskite films during annealing, preventing them from evaporating and passivating crystal growth regions. Cai et al. studied the effect of three polymers on perovskites-HTL interface modification, including hydrophilic PEG, thermoplastic poly (methylmethacrylate) (PMMA), and poly [2-methoxy-5-(2-ethylhexyloxy)-1,4-pheny-lenevinylene] (MEH-PPV) semiconductor. Based on their analysis of the modified perovskite films, it was found that the modified perovskite films were more tetrahedral with lower surface roughness and exhibited enhanced photovoltaic characteristics [35]. Our previous study showed that localized defects can be passivated through Lewis acid–base interactions to improve photodetection performance [36]. Interestingly, hygroscopic PEG protects the perovskite layer from moisture, resulting in exceptionally stable perovskite films and devices [37]. Despite the progress in enhancing the stability of perovskite solar cells in a humid environment, there is a lack of study on the improvement of thermal stability for the hybrid perovskite films and the associated solar cells with the use of PEG polymers.

In this study, we demonstrate that a mixture of crystalline thermoplastic additives, polyethylene glycol (PEG), and polyethylene oxide (PEO) delivers a high-performance and thermally stable perovskite solar cell. As a conclusion, PEO + PEG mixture treatment results in a high-performance inverted perovskite solar cell with a high efficiency of 18.55%. Moreover, thermoplastic PEO and/or PEO + PEG mixtures with high molecular weights can play a role as a shield to stabilize the perovskite texture under heat attack; the unencapsulated devices with PEO + PEG modification showed enhanced thermal stability, as

they maintained 71% of their initial efficiencies after 120 h of presence at 81 °C in ambient air with a relative humidity (RH) of 50–60% in dark conditions. However, the efficiencies of the untreated devices sharply decreased to 10% of their initial values after only 48 h under the same test conditions. Overall, this treatment provides a viable way to increase the thermal stability of perovskite solar cells.

2. Experimental Section

2.1. Materials

Methylammonium iodide (MAI, 99.99%), lead iodide (PbI_2, 99.99%), bathocuproine (BCP, 99%), and Poly [bis (4-phenyl) (2,4,6-trimethylphenyl) amine (PTAA) were purchased from Xi'an Polymer Light Technology Corp. Polyethylene oxide (PEO, 100,000 MW) and polyethylene glycol (PEG, 12,000 MW) were purchased from Alfa Aesar. N, N-Dimethylformamide (DMF, 99.8%), chlorobenzene (CB, 99.8%), and isopropanol (IPA, 99.5%) were purchased from Sigma-Aldrich. Buckminsterfullerene (C_{60}, 99%) was purchased from Nano-C. Silver (Ag, ≥99.99%) was purchased from ZhongNuo Advanced Material (Beijing, China). Indium tin oxide coated glass (ITO glass) was bought from Huanan Xiangcheng Technology Co., Ltd. (Changsha, China).

2.2. Film and Device Fabrication

Cleaning of indium tin oxide (ITO) glasses was carried out successively with detergent, water, acetone, and isopropanol and then dried at 70 °C. A further 20 min UV-ozone treatment was applied to the as-treated ITO substrates to increase their hydrophilicity. The substrates were then transferred to an N_2-filled glove box. ITO substrates were spin-coated with PTAA solution (5 mg/mL in toluene) at 4000 rpm for 30 s, followed by annealing at 100 °C for 10 min. The $MAPbI_3$ films were prepared by a two-step technique. Three different types of solution were prepared: 1. 1.2 M PbI_2, and 0.2 M MAI in DMF solvent with different PEG concentration ratios (0, 0.5, 1, and 2 mg/mL); 2. 1.2 M PbI_2 and 0.2 M MAI in DMF solvent with different PEO concentration ratios (0, 0.5, 1, and 2 mg/mL); 3. A combination of PEO + PEG in different ratios, including (PEO 0.5 mg + PEG 0.5 mg), (PEO 1 mg + PEG 1 mg), and (PEO 2 mg + PEG 2 mg), was added to 1.2 M PbI_2 and 0.2 M MAI in 1 mL DMF solvent. All of these solutions were spin-coated onto PTAA at 6000 rpm for 20 s. The $MAPbI_3$ perovskite films were formed by dropping the MAI solution (40 mg/mL in IPA) onto the PbI_2-rich substrates at 4000 rpm, followed by 30 min of annealing at 100 °C. Then, thermal evaporation was used to fabricate C_{60} (20 nm), BCP (7 nm), and Ag (80 nm). The active area of the device was defined as 0.08 cm^2.

2.3. Instrumentation

Current density-voltage (*J-V*) curves were measured without mask using a Keithley 2450 Source Meter under AM 1.5G irradiation (100 mW/cm^2) with a xenon-lamp solar simulator (Newport Oriel 66902). For the EQE curves, a quantum efficiency measurement system (Enli Technology) was used in air without encapsulation. A Bruker D8 ADVANCE X-ray diffractometer and a Cu-K radiation source (λ = 1.5418 Å) were applied to acquire the X-ray diffraction (XRD) patterns. The surface and cross-sectional morphological photos were captured with a Navi Innovation scanning electron microscope and Helios Nano Lab G3 UC scanning electron microscope, respectively. The surface composition of the perovskite was studied by X-ray photoelectron spectroscopy (XPS) using AXIS SUPRA+.

3. Results and Discussion

In principle, PEO and PEG polymers have the same molecular formula, and their names are defined based on their molecular weight (MW). PEG is typically used for MWs of less than 20,000, whereas PEO is used for MWs of above 20,000. In order to investigate the effect of the molecular weight of polyethylene glycol on the photovoltaic performance of $MAPbI_3$ perovskite solar cells, PEG (MW 12,000), PEO (MW 100,000), and a mixture of PEO and PEG (PEO + PEG; weight ratio, 1:1; the PEO + PEG with a molecular weight

between PEG and PEO) were introduced as additives into the step-one PbI_2 solution to modify the $MAPbI_3$ perovskites. By using these additives, the effect of different molecular weights of the polymers on the performance of perovskite solar cells can be studied. The top-view scanning electron microscopy (SEM) images of ITO/PTAA/$MAPbI_3$ films fabricated without and with PEG, PEO, and PEO + PEG are shown in Figures 1a–d and S1. SEM photographs demonstrate that perovskite grains are uniform and in good contact, and no pinholes are observed in all the perovskite films. Meanwhile, it is found that the grain sizes of the perovskite films are significantly reduced after modifying the $MAPbI_3$ perovskite with PEG, PEO, and PEO + PEG polymers. In addition, the effect of a PEO + PEG mixture on the morphology of a different perovskite composition ($MAPbI_xCl_{3-x}$) was investigated, and we find that the grain size of the $MAPbI_xCl_{3-x}$ perovskite film is also significantly reduced after introducing a PEO + PEG mixture (Figure S2). It is reported that the interactions between hydroxy groups of PEG (or PEO) and lead ions can form more nucleation sites during the perovskite crystallization process, thereby generating the smaller grains [38]. According to our previous work, the molecular weight of poly (ethylene glycol) additives affected the perovskite crystal size due to the steric effect of polymeric additions [36]. Meanwhile, the steric effect of PEG-related polymers with long ligands could hinder perovskite crystallization and form a compact and uniform perovskite film with smaller grains. Moreover, PEG and PEO increase the surface energies of the $MAPbI_3$ perovskites, contributing to the total Gibbs energy; the smaller grain sizes are thus expected to stabilize the perovskite phase of the $MAPbI_3$ active layers. This approach has also been found to be effective when combined with polyethylene glycol modifications, which increases the perovskite film's tolerance to moisture [38]. It should be pointed out that an excess of small grains is not beneficial to form the high-quality film [39]; thus, a better perovskite film can be expected to form when employing PEO + PEG modifiers with a suitable molecular weight.

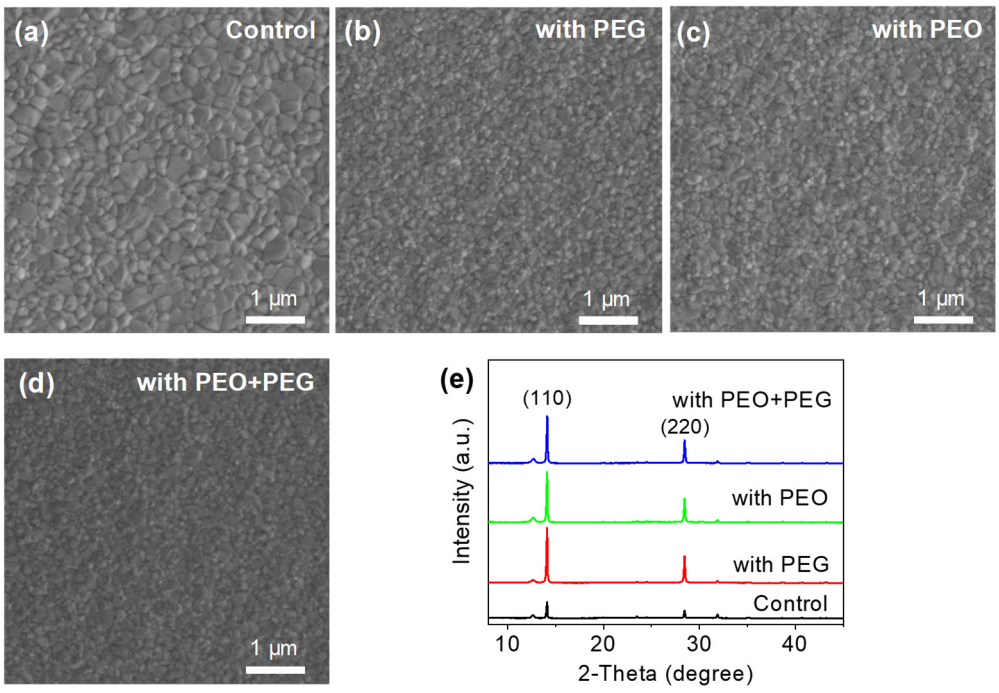

Figure 1. SEM images of (**a**) the control perovskite film, (**b**) PEG treated perovskite film, (**c**) PEO treated perovskite film, and (**d**) PEO + PEG treated perovskite films. (**e**) XRD patterns of the control perovskite films without and with PEG, PEO, and PEO + PEG mixture treatment.

Furthermore, the impact of PEG, PEO and PEO + PEG on the perovskite crystal structure was further investigated by recording X-Ray diffraction (XRD) patterns, as displayed in Figure 1e. All the samples showed two characteristic peaks at 14.0° and 28.3°, which are

assigned to the (110) and (220) lattice planes of the tetragonal $MAPbI_3$ perovskite crystal, and a higher crystallinity is found in the modified perovskite films based on the enhanced intensities at both the (110) and (220) planes, leading to better performance of the perovskite solar cells. This increase in intensity of characteristic peaks is mainly due to the formation of Lewis base reactions between PEG (and PEO) with hydroxy groups and the uncoordinated Pb^{2+} in $MAPbI_3$ perovskite. Such a strong interaction is expected to increase the activation energy of nucleation, which is able to slow down perovskite crystal growth to improve the crystallinity of the perovskite films with a preferred orientation, forming a high-quality perovskite film with low nonradiative recombination defects. In addition, a small peak at 12.5° is also found in these perovskite films, indicating an excess of PbI_2. A small amount of PbI_2 in the $MAPbI_3$ perovskite is expected to improve the optoelectronic performance of the perovskite film [40].

We then investigated the effect of the molecular weight of polyethylene glycol on the thermal stability of the perovskite films at 85 °C by recording XRD patterns. As shown in Figure 2a, the control perovskite film showed a large increase in two additional peaks at 12.6° and 38.6° with increasing heating time, which correspond to the (001) and (003) planes of the hexagonal PbI_2 phase. Meanwhile, distinct PbI_2 was also observed in the perovskite film with PEG modification over time (Figure 2b). However, only a small PbI_2 product was observed in the PEO and PEO + PEG-treated perovskite films under the same thermal stability conditions (Figure 2c,d). This indicates that PEO and PEO + PEG can improve the endurance of the $MAPbI_3$ perovskite film against heat, which should be attributable to the usage of thermoplastic PEO and/or PEO + PEG with high molecular weight. The thermal stability of perovskite solar cells with PEO + PEG modification is attributed to the thermoplastic properties of the mixture, which enable the device to remain stable even when exposed to high temperatures, ensuring its long-term performance. The reaction between the hydroxyl group of PEO + PEG and the uncoordinated Pb^{2+} in $MAPbI_3$ perovskite forms a protective layer that shields it from heat attack. All of these factors contribute to the enhanced thermal stability of perovskite solar cells.

The planar heterojunction perovskite solar cells were constructed with a structure of poly [bis (4-phenyl) (2,4,6-trimethylphenyl)amine] (PTAA)/$MAPbI_3$ perovskite/fullerene (C_{60})/2,9 dimethyl-4,7-diphenyl-1,10-phenanthroline (BCP)/Ag to investigate the influence of PEO and PEG on the device performance, as shown in Figure 3a. Figure 3a displays the cross-sectional SEM image of the realistic device, suggesting a dense and uniform layered morphology. To further investigate the effect of these additives on device performance, we optimized the concentration ratio of PEG-only (0, 0.5, 1 and 2 mg/mL), PEO-only (0, 0.5, 1, and 2 mg/mL), and a combination of PEO + PEG (0.5 + 0.5, 1 + 1, and 2 + 2) mg in 1 mL DMF. As shown in Figure 3b, the pristine device showed a PCE of 17.21%, along with an open circuit voltage (V_{OC}) of 1.051 V, a short-circuit current density (J_{SC}) of 22.73 mA/cm^2, and a fill factor (FF) of 0.72. After the PEG-only (0.5) modification, the device showed a PCE of 17.35%, along with a V_{OC} of 1.067 V, a J_{SC} of 22.22 mA/cm^2, and an FF of 0.72. When the amount of PEG was increased to 1 mg, the device exhibited a higher PCE of 17.74%, along with a V_{OC} of 1.070 V, a J_{SC} of 23.04 mA/cm^2, and an FF of 0.71. However, the PEG (2) device only showed a lower PCE of 17.25%, a V_{OC} of 1.070 V, a J_{SC} of 22.52 mA/cm^2, and an FF of 0.71. Similarly, as illustrated in Figure 3c, the untreated device showed a PCE of 17.42%, along with a V_{OC} of 1.051 V, a J_{SC} of 22.03 mA/cm^2, and an FF of 0.70. After the PEO (0.5) modification, the device showed a PCE of 17.28%, a V_{OC} of 1.064 V, a J_{SC} of 21.93 mA/cm^2, and an FF of 0.73. The PEO (1) device showed a PCE of 17.62%, a V_{OC} of 1.081 V, a J_{SC} of 23.54 mA/cm^2, and an FF of 0.68. Lastly, the PEO (2) device showed a PCE of 17.07%, a V_{OC} of 1.083 V, a J_{SC} of 23.18 mA/cm^2, and an FF of 0.67. Furthermore, the optimization of the concentration ratio of PEO + PEG-based devices was also investigated. As illustrated in Figure 3d, the control device showed a PCE of 18.14%, a V_{OC} of 1.056 V, a J_{SC} of 23.12 mA/cm^2, and an FF of 0.73. After the modification of PEO + PEG (0.5 + 0.5), the device showed an improved PCE of 18.44%, a V_{OC} of 1.064 V, a J_{SC} of 23.26 mA/cm^2, and an FF of 0.73. Specifically, the device with PEO + PEG (1 + 1) showed

a further increase in PCE of 18.76%, along with a V_{OC} of 1.061 V, a J_{SC} of 23.34 mA/cm^2, and an FF of 0.75. However, the device with PEO + PEG (2 + 2) showed a decreased PCE of 17.74%, with a V_{OC} of 1.069 V, a J_{SC} of 22.72 mA/cm^2, and an FF of 0.72. Thus, the photovoltaic performance of PEG-, PEO-, and PEO + PEG-treated devices was evaluated with an optimized ratio of 1 mg, 1 mg, and 1 mg + 1 mg in a 1 mL precursor solution, respectively. In addition, statistical analysis further confirmed the optimization of these PEG, PEO, and PEO + PEG concentrations to modify the solar cells based on $MAPbI_3$ perovskites (Figure S3).

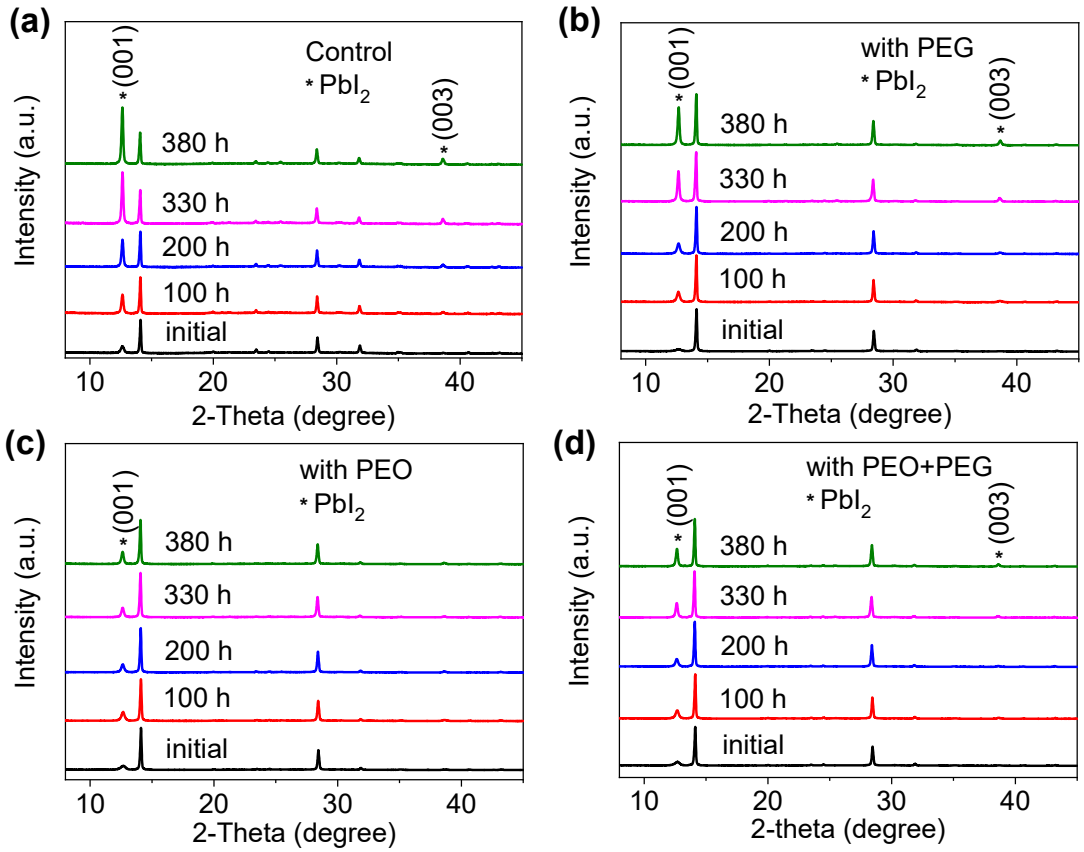

Figure 2. XRD patterns of the perovskite film without (**a**) and with (**b**) PEG, (**c**) PEO, and (**d**) PEO + PEG treatment before and after thermal stability at 85 °C. * represent the characteristic peaks of PbI_2.

The comparison of photovoltaic performances between the control device and PEO-, PEG-, and PEO + PEG-treated devices is shown in Figure 3e, and the relevant parameters (average values) are listed in Table 1. The control device showed a PCE of 18.36%, along with a V_{OC} of 1.058 V, a J_{SC} of 23.65 mA/cm^2, and an FF of 0.72. After modifying the perovskites with PEG-only and PEO-only, the efficiencies decreased to 17.33% and 16.56%, mainly due to the lower J_{SC} of 22.02 mA/cm^2 and 22.66 mA/cm^2, respectively. However, the PSC modulated by the PEO + PEG mixture yielded a higher PCE of 18.70%, accompanied by a V_{OC} of 1.066 V, a higher J_{SC} of 23.62 mA/cm^2, and a higher FF of 0.73. Additionally, the PEO + PEG mixture was further used to decorate the $MAPbI_xCl_{3-x}$-based device, as shown in Figure S4 and Table S1. We found that PEO + PEG can also improve the device performance of the solar cell based on $MAPbI_xCl_{3-x}$ perovskite. These results indicate that the addition of PEO + PEG to the perovskite layer can improve the photovoltaic performance of devices based on different perovskite compositions. The variation in current densities for these devices was further confirmed by the external quantum efficiency (EQE) spectra, as shown in Figure 3f. The EQE spectra demonstrated that the integrated J_{SC} values of the PSCs correlated with their J_{SC} values from the *J-V* test results. The current density of PSCs decreased after decorating the perovskite films with PEO only and PEG only and

increased when PEO was blended with PEG. In addition, statistical analysis of 20 devices further suggested that all the performance parameters were reduced when the devices were modified only with PEO and PEG. On the contrary, these parameters of the devices were raised after employing the PEG + PEO mixture, as compared to the control, PEG-, and PEO-treated devices (Figure 3g,h). This improvement in performance was demonstrated by the transformed data represented in Figure 3g,h, which show a significant increase in the performance parameters of the PEO + PEG-treated device. In addition, after modifying the perovskites with PEO and PEO + PEG polymers, the current density of the devices decreased from 23.65 to 21.66 and 23.62 mA/cm^2, respectively. This is mainly due to the insulating property and steric effect of polymer materials. In addition, PEO with a higher molecular weight can show a stronger steric effect than PEO + PEG. Strong steric effects can hinder charge extraction and transport, reducing the currents and device efficiencies. However, PEO + PEG with a suitable molecular weight reduces defects in the perovskite film through Lewis base reactions, while having weaker steric effects compared to PEO. It is concluded that independent PEO and PEG can have a negative impact on enhancing the device performance, whereas the combination of PEO and PEG can have a beneficial effect and improve the photovoltaic performance of perovskite solar cells.

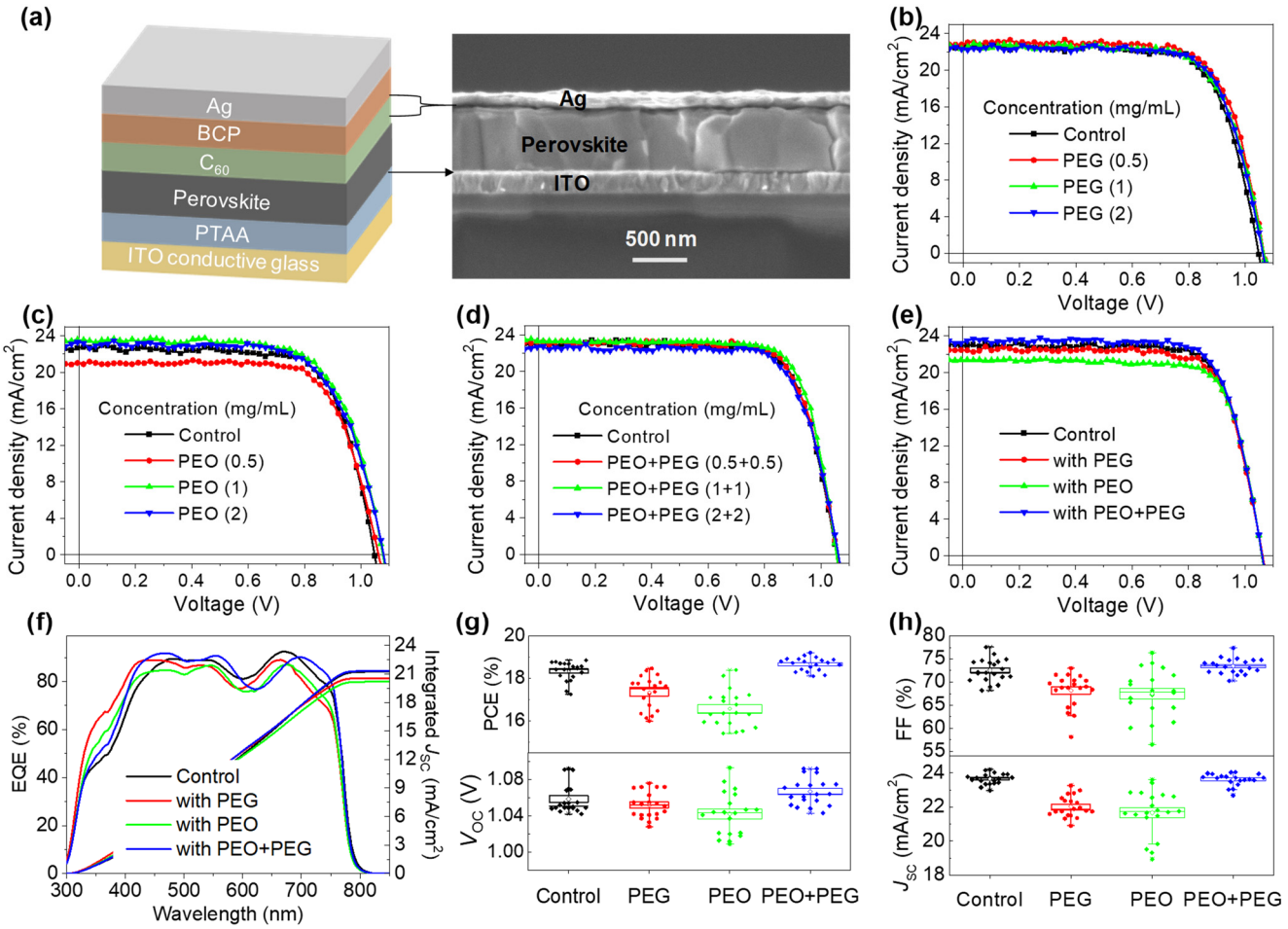

Figure 3. (**a**) Device configuration and cross-sectional SEM image of the real device. *J-V* curves of the perovskite solar cells based on different concentrations of (**b**) PEG (0, 0.5, 1, and 2 mg/mL), (**c**) PEO (0, 0.5, 1, and 2 mg/mL), and (**d**) PEO + PEG (0, 0.5 + 0.5, 1 + 1, and 2 + 2 mg/mL). (**e**) *J-V* curves, (**f**) EQE spectra and statistical distribution of (**g**) PCE and V_{OC} and (**h**) FF and J_{SC} of the PSCs with and without PEG, PEO, and PEO + PEG mixture.

Table 1. Photovoltaic parameters (average values) of the PSCs without and with PEG, PEO, and PEO + PEG treatment.

Devices	V_{OC} (V)	J_{SC} (mA/cm^2)	FF	PCE (%)
Control	1.058	23.65	0.72	18.36
With PEG	1.052	22.02	0.68	17.33
With PEO	1.042	21.66	0.67	16.56
With PEO + PEG	1.066	23.62	0.73	18.70

In addition, as a result of the PEO + PEG (1 mg + 1 mg) mixture allowing improvement in the device performance, rather than the individual PEO and PEG, we further investigated the thermal stability of the device without encapsulation based on the ISOS-D-2 protocol [41], as shown in Figure 4a. The device containing the PEO + PEG mixture showed excellent thermal stability, with 71% of initial PCE values retained after 120 h under heating stress at 85 °C in ambient air with a RH of 50–60% in dark conditions. In comparison, the control device efficiencies decreased to only 10% of their initial values after only 48 h under the same test conditions. Additionally, the *J-V* curves of the devices with and without the PEO + PEG mixture before and after thermal treatment in ambient air are also shown in Figure 4b. It was further confirmed that the combination of PEO and PEG plays an imperative role in improving the thermal stability of perovskite solar cells, as the PCE for the control device sharply dropped from 15.49% to 1.58% after only 48 h of thermal treatment at 85 °C, while the PCE for the PEO + PEG-based device dropped from 16.08% to 11.72% after 120 h. These results suggest that the PEO + PEG mixture was effective in protecting the device from deterioration under high temperature and humid conditions. The ability of the PEO + PEG mixture to maintain its PCE values for extended periods of thermal storage demonstrates its potential for practical application. This is an important characteristic when it comes to the development of devices for use in solar energy applications.

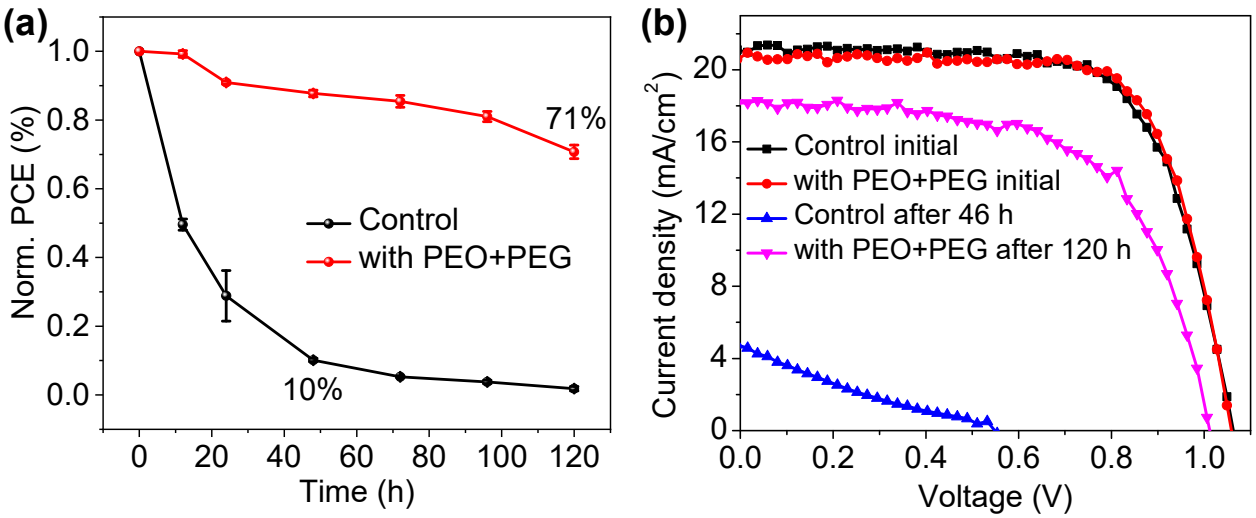

Figure 4. (**a**) Evolution of device efficiencies under heating stress at 85 °C in ambient air with a RH of 50–60% in dark conditions. (**b**) *J-V* curves of the devices with and without PEO + PEG before and after thermal stability.

X-ray photoelectron spectroscopy (XPS) was performed to reveal the element composition on the perovskite surface and clarify the interaction between the PEO + PEG mixture and perovskite. As shown in Figure 5a, a characteristic peak for O 1s was observed at a binding energy of 529.1 eV in pure perovskite, while the peak intensity was much higher and shifted to 529.7 eV when PEO + PEG was added to the perovskite film, suggesting the existence of oxygen atoms derived from PEO and PEG. In addition, from Figure 5b, we observed that the two signals of Pb $4f_{7/2}$ and Pb $4f_{5/2}$ were located at 138.4 and 143.3 eV,

respectively, for pure perovskite film. When the PEO + PEG mixture was added to the perovskite film, Pb $4f_{7/2}$ and Pb $4f_{5/2}$ were shifted to lower binding energies of 138.2 and 143.1 eV, respectively. This means that the positive charge of the Pb^{2+} ion in perovskite was lowered, which may be ascribed to the lone pair electron of the O element in PEO and PEG contributing to the 6p empty orbital of Pb^{2+}, indicating a strong interaction between PEO + PEG and perovskite. Such interaction allows for reduced trap states. Due to their nonvolatile features, PEO and PEG polymers remain predominantly at the grain boundaries during the thermal annealing process. They act as scaffolds at the grain boundaries to improve the durability of the perovskite against heat attack through the Lewis base reactions. Furthermore, perovskite film is shielded from degradation by thermoplastic PEO + PEG molecules, as illustrated in Figure 5c, which considerably improves the device's stability and contributes to its overall performance.

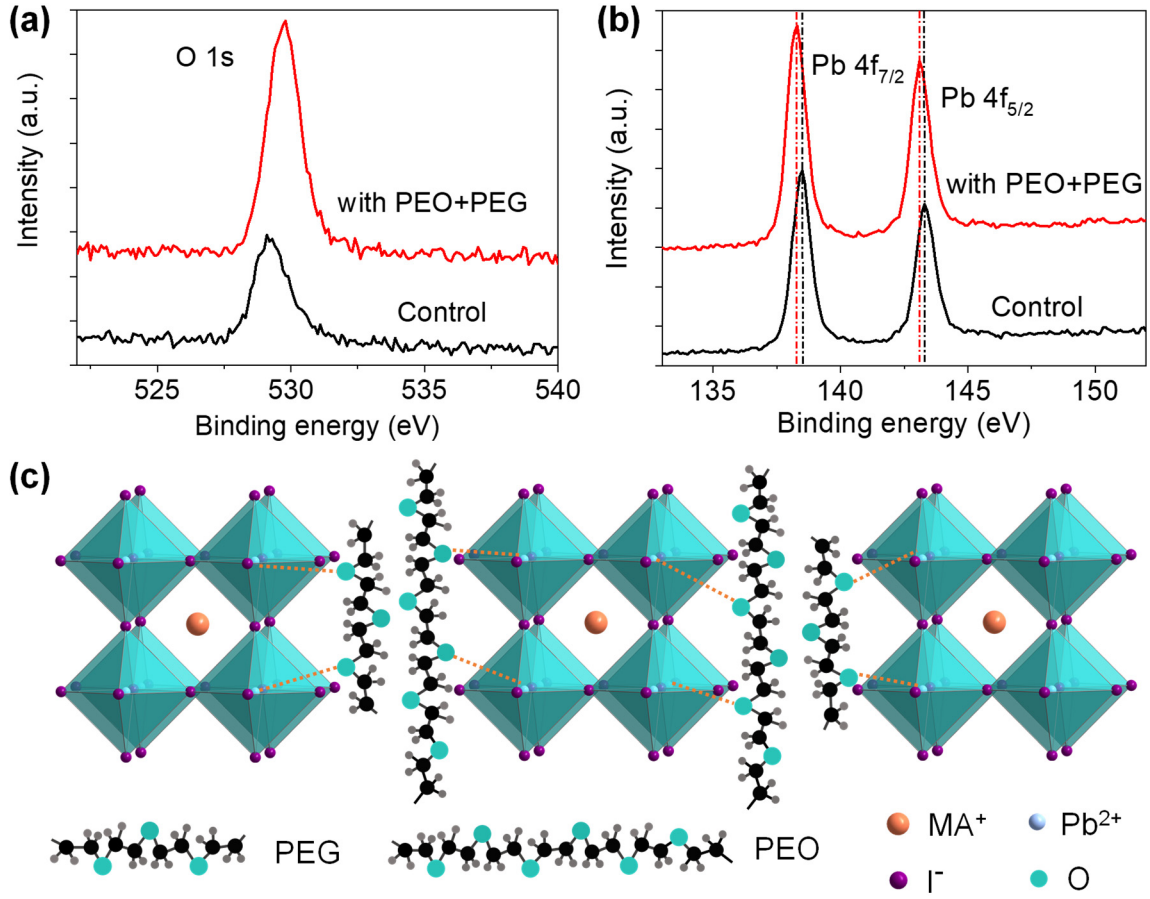

Figure 5. XPS spectra of (**a**) O 1s and (**b**) Pb 4f. (**c**) Schematic diagram of $MAPbI_3$ and PEO + PEG molecules protecting it from breakdown.

4. Conclusions

Our study demonstrated that a small quantity of the PEO + PEG mixture can be utilized as an additive in the preparation of efficient and stable perovskite solar cells. The incorporation of the PEO + PEG mixture into the $MAPbI_3$ perovskite improved device efficiency rather than individual PEO or PEG polymers. As a result of the thermoplastic shield and the Lewis base–acid reactions between the hydroxy groups in the PEO + PEG mixture and the uncoordinated Pb^{2+} in $MAPbI_3$ perovskites, PEO + PEG-based PSCs exhibit increased thermal stability at 85 °C in ambient air compared to the control device. Thus, this approach could be employed to stabilize different kinds of perovskite-based photoelectric device topologies.

Supplementary Materials: The following supporting information can be downloaded at: https://www.mdpi.com/article/10.3390/en16093621/s1, Figure S1: SEM images of the control $MAPbI_3$ perovskite film, PEG treated $MAPbI_3$ perovskite film, PEO treated $MAPbI_3$ perovskite film and PEO+PEG treated $MAPbI_3$ perovskite films; Figure S2: SEM images of $MAPbI_xCl_{3-x}$ perovskite film without and with PEO+PEG treatment; Figure S3: Statistical distribution of PCE, V_{OC}, FF and J_{SC} of the PSCs with different concentrations of PEG (0, 0.5, 1, and 2 mg/mL), PEO (0, 0.5, 1, and 2 mg/mL), and PEO+PEG (0, 0.5 + 0.5, 1 + 1, and 2 + 2 mg/mL); Figure S4: *J-V* curves of the PSCs based on $MAPbI_xCl_{3-x}$ before and after PEO+PEG treatment; Table S1: Photovoltaic parameters of the $MAPbI_xCl_{3-x}$ PSCs without and with PEO+PEG treatment.

Author Contributions: Z.U. and B.Y. designed the experiments and wrote the original draft of this manuscript; J.R., E.S. and B.Y. revised and confirmed the manuscript, B.Y. and J.R. offered financial support. All authors have read and agreed to the published version of the manuscript.

Funding: B.Y. thanks the financial support from the National Natural Science Foundation of China (62004066) and the research fund for the central universities. J.R. thanks the financial support from the Jiebang Guashuai Project of Changsha City (Grant No. kq2301002) and the research fund for the central universities.

Data Availability Statement: Data will be made available on request.

Conflicts of Interest: The authors declare no conflict of interest.

References

1. Stranks, S.D.; Eperon, G.E.; Grancini, G.; Menelaou, C.; Alcocer, M.J.P.; Leijtens, T.; Herz, L.M.; Petrozza, A.; Snaith, H.J. Electron-Hole Diffusion Lengths Exceeding 1 Micrometer in an Organometal Trihalide Perovskite Absorber. *Science* **2013**, *342*, 341–344. [CrossRef]
2. Noh, J.H.; Im, S.H.; Heo, J.H.; Mandal, T.N.; Seok, S.I. Chemical management for colorful, efficient, and stable inorganic–organic hybrid nanostructured solar cells. *Nano Lett.* **2013**, *13*, 1764–1769. [CrossRef] [PubMed]
3. Yoo, J.J.; Seo, G.; Chua, M.R.; Park, T.G.; Lu, Y.; Rotermund, F.; Kim, Y.-K.; Moon, C.S.; Jeon, N.J.; Correa-Baena, J.-P.; et al. Efficient perovskite solar cells via improved carrier management. *Nature* **2021**, *590*, 587–593. [CrossRef] [PubMed]
4. Yang, T.C.-J.; Fiala, P.; Jeangros, Q.; Ballif, C. High-Bandgap Perovskite Materials for Multijunction Solar Cells. *Joule* **2018**, *2*, 1421–1436. [CrossRef]
5. Kojima, A.; Teshima, K.; Shirai, Y.; Miyasaka, T. Organometal Halide Perovskites as Visible-Light Sensitizers for Photovoltaic Cells. *J. Am. Chem. Soc.* **2009**, *131*, 6050–6051. [CrossRef]
6. Jiang, Q.; Zhao, Y.; Zhang, X.; Yang, X.; Chen, Y.; Chu, Z.; Ye, Q.; Li, X.; Yin, Z.; You, J. Surface passivation of perovskite film for efficient solar cells. *Nat. Photon.* **2019**, *13*, 460–466. [CrossRef]
7. Wang, L.; Zhou, H.; Hu, J.; Huang, B.; Sun, M.; Dong, B.; Zheng, G.; Huang, Y.; Chen, Y.; Li, L.; et al. A Eu^{3+}-Eu^{2+} ion redox shuttle imparts operational durability to Pb-I perovskite solar cells. *Science* **2019**, *363*, 265–270. [CrossRef] [PubMed]
8. Jung, E.H.; Jeon, N.J.; Park, E.Y.; Moon, C.S.; Shin, T.J.; Yang, T.-Y.; Noh, J.H.; Seo, J. Efficient, stable and scalable perovskite solar cells using poly(3-hexylthiophene). *Nature* **2019**, *567*, 511–515. [CrossRef] [PubMed]
9. National Renewable Energy Laboratory (NREL). Best Research-Cell Efficiency Chart. Available online: https://www.nrel.gov/pv/cell-efficiency.html (accessed on 10 March 2023).
10. Leijtens, T.; Eperon, G.E.; Noel, N.K.; Habisreutinger, S.N.; Petrozza, A.; Snaith, H.J. Stability of Metal Halide Perovskite Solar Cells. *Adv. Energy Mater.* **2015**, *5*, 1500963. [CrossRef]
11. Schoonman, J. Organic–inorganic lead halide perovskite solar cell materials: A possible stability problem. *Chem. Phys. Lett.* **2015**, *619*, 193–195. [CrossRef]
12. Giustino, F.; Snaith, H.J. Toward Lead-Free Perovskite Solar Cells. *ACS Energy Lett.* **2016**, *1*, 1233–1240. [CrossRef]
13. Bryant, D.; Aristidou, N.; Pont, S.; Sanchez-Molina, I.; Chotchunangatchaval, T.; Wheeler, S.; Durrant, J.R.; Haque, S.A. Light and oxygen induced degradation limits the operational stability of methylammonium lead triiodide perovskitesolar cells. *Energy Environ. Sci.* **2016**, *9*, 1655–1660. [CrossRef]
14. Leguy, A.M.; Hu, Y.; Campoy-Quiles, M.; Alonso, M.I.; Weber, O.J.; Azarhoosh, P.; Van Schilfgaarde, M.; Weller, M.T.; Bein, T.; Nelson, J.; et al. Reversible hydration of $CH_3NH_3PbI_3$ in films, single crystals, and solar cells. *Chem. Mater.* **2015**, *27*, 3397–3407. [CrossRef]
15. Wei, J.; Wang, Q.; Huo, J.; Gao, F.; Gan, Z.; Zhao, Q.; Li, H. Mechanisms and Suppression of Photoinduced Degradation in Perovskite Solar Cells. *Adv. Energy Mater.* **2020**, *11*, 2002326–2002356. [CrossRef]
16. Khenkin, M.V.; Anoop, M.K.; Visoly-Fisher, I.; Kolusheva, S.; Galagan, Y.; Di Giacomo, F.; Vukovic, O.; Patil, B.R.; Sherafatipour, G.; Turkovic, V.; et al. Dynamics of Photoinduced Degradation of Perovskite Photovoltaics: From Reversible to Irreversible Processes. *ACS Appl. Energy Mater.* **2018**, *1*, 799–806. [CrossRef]

17. Zhu, W.; Xin, G.; Scott, S.M.; Xu, W.; Yao, T.; Gong, B.; Wang, Y.; Li, M.; Lian, J. Deciphering the degradation mechanism of the lead-free all inorganic perovskite Cs2SnI6. *NPJ Mater. Degrad.* **2019**, *3*, 1–7. [CrossRef]
18. Aristidou, N.; Eames, C.; Sanchez-Molina, I.; Bu, X.; Kosco, J.; Islam, M.S.; Haque, S.A. Fast oxygen diffusion and iodide defects mediate oxygen-induced degradation of perovskite solar cells. *Nat. Commun.* **2017**, *8*, 15218–15227. [CrossRef]
19. Mohammadi, M.; Gholipour, S.; Byranvand, M.M.; Abdi, Y.; Taghavinia, N.; Saliba, M. Encapsulation Strategies for Highly Stable Perovskite Solar Cells under Severe Stress Testing: Damp Heat, Freezing, and Outdoor Illumination Conditions. *ACS Appl. Mater. Interfaces* **2021**, *13*, 45455–45464. [CrossRef]
20. Rolston, N.; Printz, A.D.; Tracy, J.M.; Weerasinghe, H.C.; Vak, D.; Haur, L.J.; Priyadarshi, A.; Mathews, N.; Slotcavage, D.J.; McGehee, M.D.; et al. Effect of Cation Composition on the Mechanical Stability of Perovskite Solar Cells. *Adv. Energy Mater.* **2017**, *8*, 1702116–1702122. [CrossRef]
21. Ha, S.R.; Jeong, W.H.; Liu, Y.; Oh, J.T.; Bae, S.Y.; Lee, S.; Kim, J.W.; Bandyopadhyay, S.; Jeong, H.I.; Kim, J.Y.; et al. Molecular aggregation method for perovskite–fullerene bulk heterostructure solar cells. *J. Mater. Chem. A* **2019**, *8*, 1326–1334. [CrossRef]
22. Chae, S.; Yi, A.; Kim, H.J. Molecular engineering of a conjugated polymer as a hole transporting layer for versatile p–i–n perovskite solar cells. *Mater. Today Energy* **2019**, *14*, 100341–100348. [CrossRef]
23. Meng, Z.; Guo, D.; Yu, J.; Fan, K. Investigation of Al_2O_3 and ZrO_2 spacer layers for fully printable and hole-conductor-free mesoscopic perovskite solar cells. *Appl. Surf. Sci.* **2018**, *430*, 632–638. [CrossRef]
24. Lao, Y.; Zhang, Y.; Yang, S.; Zhang, Z.; Yu, W.; Qu, B.; Xiao, L.; Chen, Z. Efficient Perovskite Solar Cells with Enhanced Thermal Stability by Sulfide Treatment. *ACS Appl. Mater. Interfaces* **2022**, *14*, 27427–27434. [CrossRef]
25. Zou, J.; Liu, W.; Deng, W.; Lei, G.; Zeng, S.; Xiong, J.; Gu, H.; Hu, Z.; Wang, X.; Li, J. An efficient guanidinium isothiocyanate additive for improving the photovoltaic performances and thermal stability of perovskite solar cells. *Electrochim. Acta* **2018**, *291*, 297–303. [CrossRef]
26. Tang, X.; Chen, M.; Jiang, L.; Li, M.; Tang, G.; Liu, H. Improvements in Efficiency and Stability of Perovskite Solar Cells Using a Cesium Chloride Additive. *ACS Appl. Mater. Interfaces* **2022**, *14*, 26866–26872. [CrossRef] [PubMed]
27. Liao, H.; Guo, P.; Hsu, C.; Lin, M.; Wang, B.; Zeng, L.; Huang, W.; Soe, C.M.M.; Su, W.; Bedzyk, M.J.; et al. Enhanced Efficiency of Hot-Cast Large-Area Planar Perovskite Solar Cells/Modules Having Controlled Chloride Incorporation. *Adv. Energy Mater.* **2016**, *7*, 1601660–1601668. [CrossRef]
28. Liu, S.; Guan, Y.; Sheng, Y.; Hu, Y.; Rong, Y.; Mei, A.; Han, H. A Review on Additives for Halide Perovskite Solar Cells. *Adv. Energy Mater.* **2019**, *10*, 1902492–1902519. [CrossRef]
29. Afroz, M.A.; Ghimire, N.; Reza, K.M.; Bahrami, B.; Bobba, R.S.; Gurung, A.; Chowdhury, A.H.; Iyer, P.K.; Qiao, Q. Thermal Stability and Performance Enhancement of Perovskite Solar Cells Through Oxalic Acid-Induced Perovskite Formation. *ACS Appl. Energy Mater.* **2020**, *3*, 2432–2439. [CrossRef]
30. Liu, Y.; Gao, Y.; Lu, M.; Shi, Z.; Yu, W.W.; Hu, J.; Bai, X.; Zhang, Y. Ionic additive engineering for stable planar perovskite solar cells with efficiency >22%. *Chem. Eng. J.* **2021**, *426*, 130841–130847. [CrossRef]
31. Li, X.; Ke, S.; Feng, X.; Zhao, X.; Zhang, W.; Fang, J. Enhancing the stability of perovskite solar cells through cross-linkable and hydrogen bonding multifunctional additives. *J. Mater. Chem. A* **2021**, *9*, 12684–12689. [CrossRef]
32. Peng, J.; Khan, J.I.; Liu, W.; Ugur, E.; Duong, T.; Wu, Y.; Shen, H.; Wang, K.; Dang, H.; Aydin, E.; et al. A Universal Double-Side Passivation for High Open-Circuit Voltage in Perovskite Solar Cells: Role of Carbonyl Groups in Poly(methyl methacrylate). *Adv. Energy Mater.* **2018**, *8*, 1801208–1801216. [CrossRef]
33. Collavini, S.; Cabrera-Espinoza, A.; Delgado, J.L. Organic Polymers as Additives in Perovskite Solar Cells. *Macromolecules* **2021**, *54*, 5451–5463. [CrossRef]
34. Lee, K.-M.; Chan, S.-H.; Ting, C.-C.; Chen, S.-H.; Chiu, W.-H.; Suryanarayanan, V.; Hsu, J.-F.; Liu, C.-Y.; Wu, M.-C. Surfactant Tween 20 Controlled Perovskite Film Fabricated by Thermal Blade Coating for Efficient Perovskite Solar Cells. *Nanomaterials* **2022**, *12*, 2651. [CrossRef]
35. Cai, Y.; Zhang, Z.; Zhou, Y.; Liu, H.; Qin, Q.; Lu, X.; Gao, X.; Shui, L.; Wu, S.; Liu, J. Enhancing the efficiency of low-temperature planar perovskite solar cells by modifying the interface between perovskite and hole transport layer with polymers. *Electrochim. Acta* **2018**, *261*, 445–453. [CrossRef]
36. Li, J.; Zhang, G.; Zhang, Z.; Li, J.; Uddin, Z.; Zheng, Y.; Shao, Y.; Yuan, Y.; Yang, B. Defect Passivation via Additive Engineering to Improve Photodetection Performance in $CsPbI_2Br$ Perovskite Photodetectors. *ACS Appl. Mater. Interfaces* **2021**, *13*, 56358–56365. [CrossRef] [PubMed]
37. Zhao, Y.; Wei, J.; Li, H.; Yan, Y.; Zhou, W.; Yu, D.; Zhao, Q. A polymer scaffold for self-healing perovskite solar cells. *Nat. Commun.* **2016**, *7*, 10228. [CrossRef]
38. Zhang, C.; Wan, X.; Zang, J.; Liu, Q.; Fei, Y.; Yu, Z. Polymer-modified $CsPbI_2Br$ films for all-inorganic planar perovskite solar cells with improved performance. *Surfaces Interfaces* **2020**, *22*, 100809–100815. [CrossRef]
39. Jiang, L.L.; Wang, Z.K.; Li, M.; Zhang, C.C.; Ye, Q.Q.; Hu, K.H.; Lu, D.Z.; Fang, P.F.; Liao, L.S. Passivated Perovskite Crystallization via g-C3N4 for High-Performance Solar Cells. *Adv. Funct. Mater.* **2018**, *28*, 1705875–1705882. [CrossRef]

40. Roose, B.; Dey, K.; Chiang, Y.H.; Friend, R.H.; Stranks, S.D. Critical Assessment of the Use of Excess Lead Iodide in Lead Halide Perovskite Solar Cells. *J. Phys. Chem. Lett.* **2020**, *11*, 6505–6512. [CrossRef]
41. Khenkin, M.V.; Katz, E.A.; Abate, A.; Bardizza, G.; Berry, J.J.; Brabec, C.; Brunetti, F.; Bulović, V.; Burlingame, Q.; Di Carlo, A.; et al. Consensus statement for stability assessment and reporting for perovskite photovoltaics based on ISOS procedures. *Nat. Energy* **2020**, *5*, 35–49. [CrossRef]